Experiments in Fluids (2025) 66:21
https://doi.org/10.1007/s00348-024-03934-6

RESEARCH ARTICLE

Particle shadow velocimetry and its potential applications, limitations and advantages vis-à-vis particle image velocimetry

Gauresh Raj Jassal[1] · **Maxwell Song**[1] · **Bryan E. Schmidt**[1]

Received: 16 September 2024 / Revised: 26 November 2024 / Accepted: 27 November 2024 / Published online: 8 January 2025

Abstract

Particle image velocimetry (PIV) is an established velocimetry technique in experimental fluid mechanics that involves determining a fluid flow velocity field from the motion of tracer particles illuminated by a laser sheet. The necessity of laser illumination poses challenges in certain applications and is a potential entry barrier due to its high cost and safety considerations. A laser-free alternative to PIV is particle shadow velocimetry (PSV), which uses images of the shadows cast by the particles on the camera sensor under back-illumination, instead of the Mie scattering signal produced by laser illumination. This study aims to compare various aspects of PSV such as depth of field, seeding density, type of illumination required, particle size, image filtering, cost-effectiveness and limitations with those of PIV. PSV and PIV measurements are taken in the wake of a flow past a cylinder and in a boundary layer developing over a flat plate. It is found that PSV is capable of achieving equivalent accuracy to PIV and is a viable alternative to PIV in certain applications where light sheet illumination creates experimental challenges.

1 Introduction

Particle image velocimetry (PIV) uses a sequence of experimental particle image data to determine the velocity fields of fluid flows and is a standard technique in fluid mechanics. The reader is referred to one of several reference texts, e.g., Raffel et al. (2018), for more information. In a traditional planar (2D) PIV setup as depicted in Fig. 1, the flow is seeded with small (O(1–10 μm)) tracer particles, and a laser sheet is used to illuminate the particles within the imaging plane. The interaction of the laser sheet with the particles causes scattering of the laser emission from the particles, and the resulting intensity signal is captured by a camera. When a pair of such images is captured within a short enough inter-frame time, the displacements of the particles from one frame to the next can be interpreted as the velocity field. A discussion of the algorithm for determining the inter-frame particle displacements is outside the scope of the present work. For a detailed treatment of this subject the reader is referred to Refs. Raffel et al. (2018); Schmidt and Sutton (2020, 2019); Stamhuis and Thielicke (2014), and Thielicke and Sonntag (2021).

The requirement of laser illumination in PIV introduces an additional layer of complexity and restrictions in experiments. For instance, the limited repetition rate of lasers of sufficient pulse energy can be a limiting factor when acquiring time-resolved particle image data. Additionally, the laser scattering off of solid surfaces poses a challenge when capturing near-wall particle motion in PIV experiments (Paterna et al. 2013). Finally, the requirement of additional optics to direct and shape the laser beam and the high cost of lasers act as entry barriers for taking fluid velocimetry measurements. Therefore, a laser-free alternative to particle imaging is desirable for certain applications. One such method is particle shadow velocimetry (PSV), proposed by Estevadeordal and Goss (2005). PSV has been applied sparingly in the literature, primarily in experiments involving flows with small length scales such as micro-channels (Hessenkemper and Ziegenhein 2018) (referred to as μ-PSV) and bubbly flows (Khodaparast et al. 2013, 2014), but whether it is able to obtain velocity measurements with the same fidelity as PIV remains an open question.

✉ Gauresh Raj Jassal
gauresh.jassal@case.edu

Maxwell Song
zhuoqing.song@case.edu

Bryan E. Schmidt
bryan.e.schmidt@case.edu

[1] Mechanical and Aerospace Engineering, Case Western Reserve University, Cleveland 44106, Ohio, USA

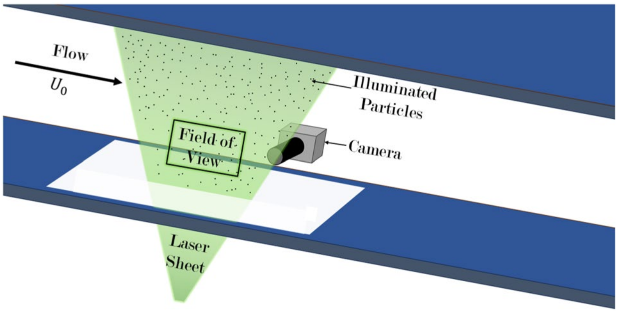

Fig. 1 A typical PIV setup

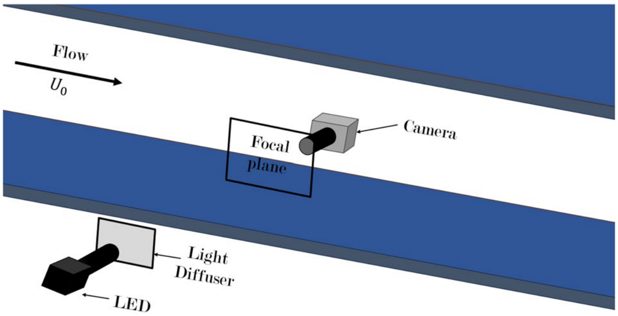

Fig. 2 A typical PSV setup

In PSV, shadows cast on the camera sensor by the tracer particles are captured instead of recording the intensity signal produced by laser–particle scattering. Collimated light from a constant or pulsed LED light source is used to backlight the seeded flow, making the system laser-free. The depth of field is controlled solely by the camera, unlike in PIV where the effective depth of field is limited to the width of the laser sheet. A schematic of a typical PSV setup is shown in Fig. 2. The setup typically consists of a light source, a collimating diffuser to create uniform collimated illumination and a camera to capture the particle images. The in-line configuration of the light source, sampling region and camera has advantages compared to PIV, where the light sheet must propagate through the test section orthogonally to the viewing perspective, requiring optical access at 90° intervals. However, it could be a drawback when considering extensions to stereoscopic or tomographic imaging. As long as the collimated light source is large enough, stereoscopic PSV could be feasible, but a tomographic arrangement would almost certainly require multiple collimated light sources, one for each camera.

A major experimental challenge in near-wall and multiphase flow particle imaging is unwanted laser scattering and reflections at surfaces (Paterna et al. 2013). As explored by Goss et al. (2007), the illumination strategy of PSV therefore provides a potential advantage for applications in these flows. Figure 3 shows an aluminum wall in a flow imaged using (a) PIV and (b) PSV, and air bubbles in water imaged using (c) PIV and (d) PSV.

Figure 3b shows that PSV does not lead to any reflections or scattering from the wall that could be detrimental to flow velocimetry. The same advantage is observed in bubbly flows, where the visibility of the air–water interface is enhanced, leading to a much more resolved flow phase field, along with the bubbles. This demonstrates a potential application of PSV where traditional particle imaging methods

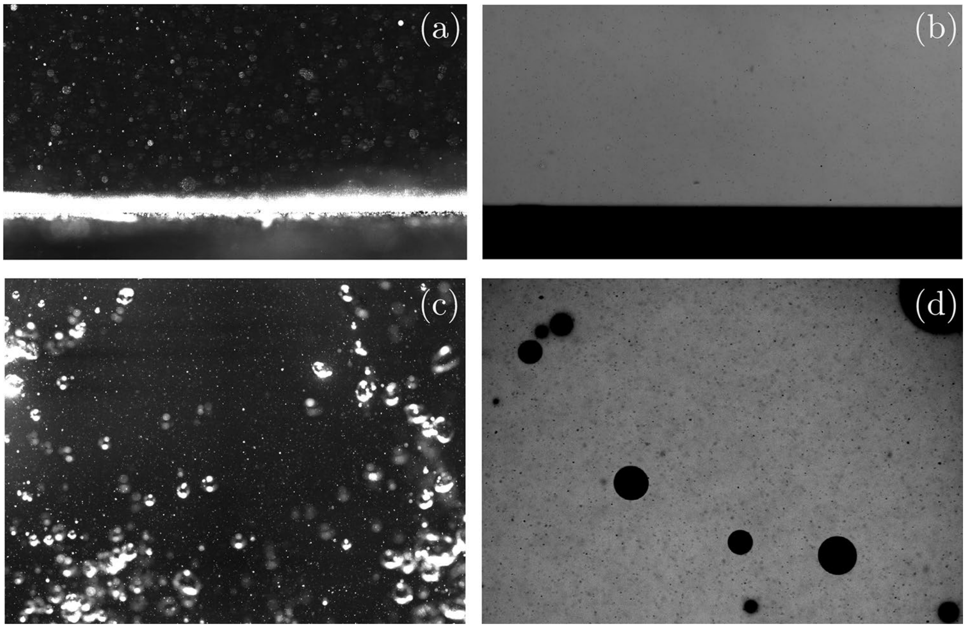

Fig. 3 Aluminum wall in a flow imaged using **a** PIV and **b** PSV, and air bubbles in water imaged using **c** PIV and **d** PSV

such as PIV do not work effectively due to inherent limitations from laser sheet imaging.

Despite its potential advantages, simplicity and cost-effectiveness, PSV has yet to be adopted in a meaningful way by researchers in the fluid mechanics community, based on an assessment of the literature. This is perhaps because its performance compared to PIV has yet to be fully assessed, and it is unclear whether PSV can obtain measurements with similar accuracy and spatial resolution to PIV. Therefore, in this study we aim to characterize various metrics and characteristics of PSV such as depth of field, seeding density, type of illumination required, particle size, image filtering, cost-effectiveness, compatibility with existing PIV processing algorithms and limitations. PIV and PSV experiments are conducted for two flow configurations: the wake of a flow past a cylinder and a boundary layer developing over a flat plate. The resulting measurements are compared to each other quantitatively and qualitatively to determine the efficacy of PSV as an alternative experimental fluid flow velocimetry measurement.

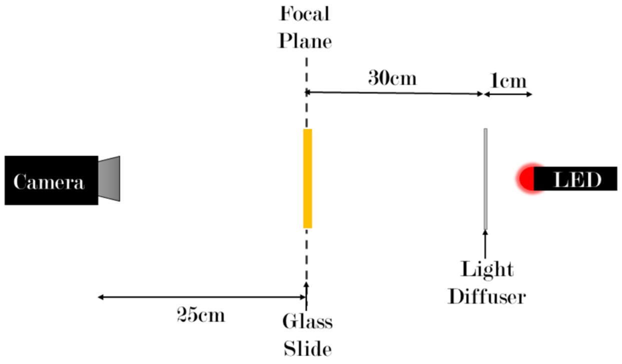

Fig. 4 A schematic of the depth of field experiment

2 Static experiments

2.1 Depth of field

In PIV imaging, the depth of field of the system is confined at most to the effective thickness of the laser sheet, typically a few millimeters. In PSV imaging, however, the depth of field is instead determined by the camera lens apparatus. To accurately characterize the effective depth of field of a PSV system, a glass slide coated with 10 µm glass sphere seeding particles of density $1.05 - 1.11\,\mathrm{g/cm^3}$ was imaged at different distances from the focal plane. A schematic of the experimental setup is provided in Fig. 4. A Photron Nova S12 equipped with a 105 mm Sigma DG macro lens with the aperture open to $f = 2.8$ was used to capture images at a resolution of 1024×1024 pixels to achieve a scaling of 40 pixels per millimeter. Figure 5 shows PSV images of the same particle (b) at the focal plane, displaced (a) 6.35 mm beyond the focal plane and (c) 6.35 mm in front of the focal plane. The in-plane focused particle casts a stronger shadow, leading to increased contrast and sharper definition of the particle image.

A curve of the minimum particle image intensity, i.e., the strongest shadow, is shown in Fig. 6a as a function of the imaging plane location, where a location of 0 mm is defined to be the location at which the particle appears to be in sharpest focus. Note that the y-axis is inverted, with lower intensity at the top. Figure 6a shows the expected increase in intensity at the particle location as the particle moves out of the focal plane of the imaging lens, leading to a weaker shadow. The full width at half maximum (FWHM) of the intensity curve shown was computed to characterize the depth of field of the system, and it was found to be 6.35 mm. This is on the larger end but within the range of typical depths of field of PIV systems for

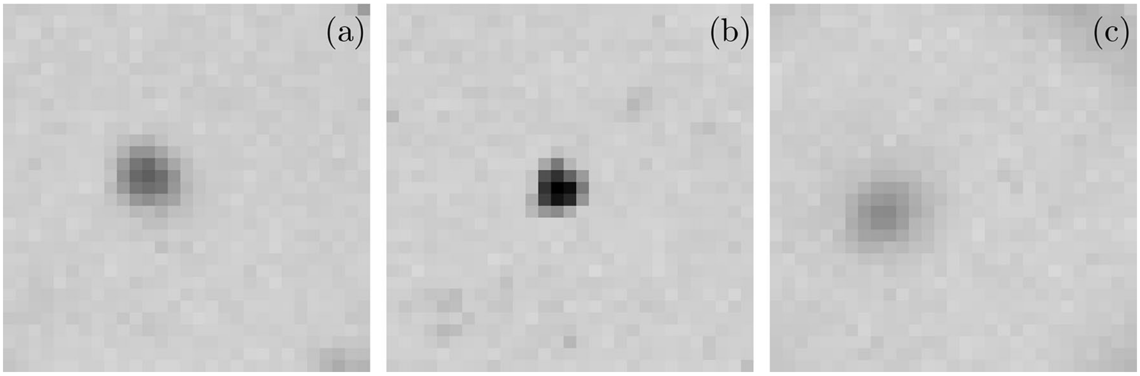

Fig. 5 PSV image of a particle captured (**a**) at a distance of 6.35 mm beyond the focal plane, (**b**) at the focal plane and (**c**) −6.35 mm from the focal plane

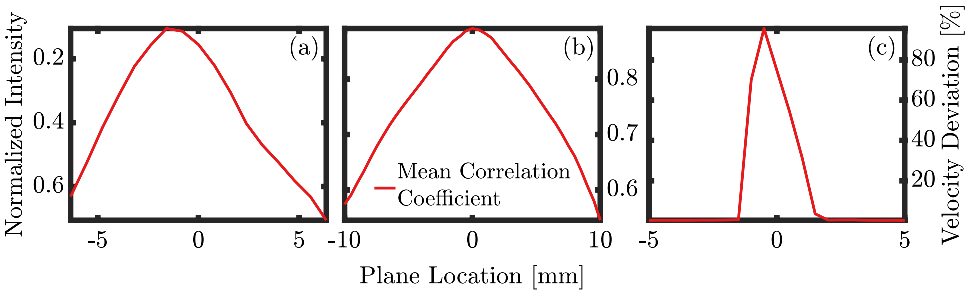

Fig. 6 **a** Normalized minimum intensity of the particle, **b** mean correlation coefficient and **c** the velocity deviation observed due to out-of-focus particles vs the distance from the focal plane

similar particle sizes and magnifications, which range from $2-8$ mm (Raffel et al. 2018).

2.2 Depth of correlation

To investigate the effect of out-of-focal-plane particles on the in-plane velocity measurements, the depth of correlation of the system was determined experimentally. Similar to the depth of field experiments described in Sect. 2.1, a glass slide coated with seeding particles was imaged at different distances from the focal plane. The glass slide was then translated by 1 mm parallel to the camera focal plane, and the imaging of the glass slide was repeated at different distances from the focal plane.

The particle displacements between the particles images in the same focal plane were then determined using PIVLab Stamhuis and Thielicke (2014); Thielicke and Sonntag (2021) with a final interrogation window size of 32×32 pixels and a 50 % overlap. Figure 6b shows the mean correlation coefficient obtained by processing the particle image data obtained at different distances from focal plane. It is observed that as particles move away from the plane, the magnitude of the correlation coefficients decays rapidly. Hence, the influence of the particles on the in-plane velocity measurements diminishes as the particles move out of the focal plane. However, it should be noted that because all the imaged particles are in the same plane in this experiment, it is likely that the magnitude of the correlation coefficient is artificially higher than what would be observed in real velocimetry experiments, as the in-plane particle image data would be dominated by particles closest to the focal plane. As a result, very few particles more than a few millimeters away from the focal plane would be expected to contribute substantially to the in-plane velocity measurements.

To further investigate the effect of the presence of both in-focus and out-of-focus particles in a PSV image, the image set obtained from these experiments was modified to include the effect of out-of-focus particles. Horizontally inverted out-of-focus images obtained at different distances from the focal plane were overlaid on top of the in-focus PSV image to obtain an image set in which the in-focus particles and out-of-focus particles move in opposite directions, providing a suitable test case in which the out-of-focus particles can significantly alter the velocity computation in the in-focus plane. These composite images were then processed using PIVLab to obtain the resulting velocity fields. The percent deviation in the velocity field obtained from the composite particle images from different distances from the focal plane with respect to the in-focus velocity was computed and is presented in Fig. 6c. It is observed that as the distance of the plane location from which the particles are added to the in-focus image increases, the deviation observed in the velocity field with respect to the in-focus velocity field decreases. At a distance of approximately ± 1.5 mm from the focal plane, the velocity deviation observed is less than 1%. Therefore, if particles are moving in a plane that is at a distance greater than 1.5 mm from the focal plane, their contribution to the velocity field computation is less than 1%. Hence, the effective total depth of correlation from this metric, which is the volume that statistically contributes to velocity measurements, is about 3 mm, which is close to PIV laser sheet thickness of $1-3$ mm.

2.3 Particle size and density

Because PSV images are produced by shadows cast by the particles on the camera sensor, the apparent particle size in an image can be smaller than that of PIV images, depending on the configuration. This is especially true for physically smaller particles, such as liquid aerosols used in PIV experiments in gases, which are typically a few hundred nanometers in diameter. This smaller particle size is coupled with the particle density in the images captured in the flow field. Figure 7a shows a raw PSV image, along with the same image preprocessed via background subtraction, median filtering and inversion as described in Sect. 3.2.1 and a PIV image taken in the same flow at the same focal plane (c). The images shown were acquired in the experimental run described in Sect. 3.1 , in the wake of a flow past a cylinder. It is observed that the effective particle density in the images is about the same between PSV and PIV for this configuration, and the apparent particle diameters are also approximately equivalent. This would likely not be the

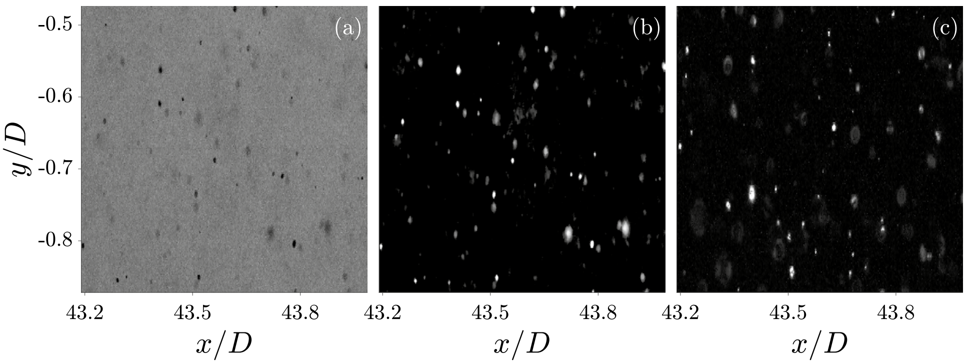

Fig. 7 **a** Raw PSV image (zoomed and contrast-enhanced for better visualization), **b** the same image preprocessed as described, **c** PIV image captured in the same flow at the same focal plane

case in systems with lower magnification or in measurements of gas flows where the tracer particles are an order of magnitude smaller.

A counterintuitive result occurs as the physical particle seeding density, i.e., the number of particles per unit volume, is increased in the flow in PSV. Beyond a certain particle density, fewer particles are visible because the light becomes diffused by the high concentration of tracers in the volume and is no longer collimated, which prevents sharp shadows from being formed. A different, but ultimately equivalent effect occurs in PIV experiments, where overseeding of the flow field leads to laser speckle due to interference and scattering (Raffel et al. 2018). Figure 8a, b shows PSV images captured in an appropriately seeded and an overseeded volume, respectively. The appropriately seeded flow has a particle seeding density of about $11\ \mathrm{g/m^3}$ leading to approximately 12 particles per square millimeter. In Fig. 8b, the light is too diffuse to produce visible shadows. The seeding density shown is about $125\mathrm{g/m^3}$ for 10-μm-diameter hollow glass spheres of density $1.05 - 1.11\ \mathrm{g/cm^3}$ in water, and the number of distinguishable particles is effectively zero.

A series of experiments were conducted where the particle seeding density was gradually increased in a fixed volume of water, carefully measuring the mass of additional particles as they were added incrementally. Experiments were conducted in a rectangular water tank with a width along the line of sight of 30 cm. Figure 8c shows the number of distinguishable particles per $\mathrm{mm^2}$ plotted against the particle concentration. As the concentration is increased, the number of distinguishable particles decreases after a critical seeding density is reached due to the scattering and light diffusion caused by the overseeded fluid. The critical seeding density is expected to depend on the width of fluid along the line of sight and other configuration-specific parameters.

3 Velocimetry experiments

3.1 Experimental setup

Both PSV and PIV systems were set up in the TRIREME water tunnel at Case Western Reserve University, which has a 1-m-long test section with a cross section of 30 cm× 30 cm. PSV and PIV images were acquired downstream of a flow past a 4.8-mm-diameter cylinder at a free stream velocity of 0.4 m/s, resulting in a Reynolds number of 1.5×10^3. Spherical hollow glass particles of diameter of 8–10 μm were seeded into the water, and 2000 statistically independent image pairs were captured at a frequency of 3.33 Hz using a Photron Nova R3-4K camera equipped with a 105 mm Sigma DG macro lens with the aperture set to $f = 2.8$ for both PSV and PIV. The camera resolution was set to 2048×1024 pixels (width × height), corresponding to

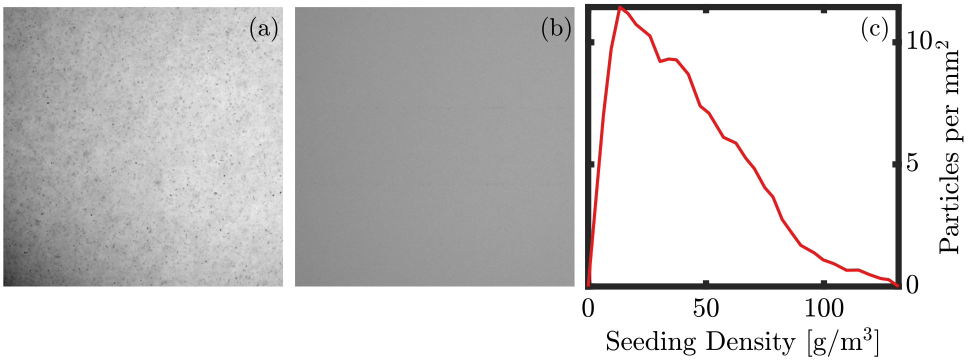

Fig. 8 **a** A raw PSV image of an appropriately seeded flow ($11\ \mathrm{g/m^3}$), **b** an overseeded flow ($130\ \mathrm{g/m^3}$) and **c** number of distinguishable particles vs particle seeding density of the flow

a field of view of 15 mm × 7 mm with an inter-frame time of 500 μs. For PSV, a continuous red LED light source was used, and the camera exposure was set to 28.6 μs, which was sufficiently short to avoid particle streaks due to overexposure. For higher flow speeds, a pulsed LED source can be used to limit the effective exposure time of the camera as in, e.g., Refs. Willert et al. (2010, 2012). The schematic of the experimental setup is shown in Fig. 9.

Both PIV and PSV imaging were performed at the same focal plane under the same experimental conditions. For PIV, the particles were illuminated by a dual-head Photonics Nd:YLF 527 nm laser where the laser sheet was formed by a diverging lens with a focal length of $f = -15$ mm.

To compare the efficacy of PSV for near-wall particle imaging, PIV and PSV were used to study the development of the boundary layer over a flat plate. The leading and trailing edges of the model are made of aluminum, whereas the flat portion of the plate is made of clear acrylic to allow the laser to transmit through the model. This has been shown to mitigate near-wall scattering in PIV (Paterna et al. 2013). The boundary layer PSV and PIV particle images were captured at a resolution of 2048 × 512 pixels with an inter-frame time of 166.7 μs, resulting in a field of view of about 13 mm × 3.5 mm. A schematic of the experimental setup is shown in Fig. 10. The particle images were captured at a distance of 45 cm from the tip of the leading edge with a free stream velocity of 0.4 m/s. The boundary layer was tripped using a rough cylindrical rod of diameter 3.125 mm placed at a distance of 7.6 cm from the leading edge, to enhance the turbulence in the near-wall flow field. The relaxation time for the particles is ≈ 5.8 μs according to the formula given by Raffel et al. (2018), leading to $\mathrm{Stk}_\eta \approx 0.1$ for the flow past a cylinder and $\mathrm{Stk}_\eta \approx 0.09$ for the BL flow. Therefore, the Stokes number for both the flows is small enough to conclude that the particles are faithfully following the fluid motion (Pope 2001).

3.2 Velocimetry results

3.2.1 Flow past A cylinder

As described in Sect. 3.1, PSV and PIV imaging were performed in the wake of a flow past a cylinder at a Reynolds number of $Re_D = 1.5 \times 10^3$. To preprocess the PSV images, a median filter is applied on a background-subtracted raw image, which is then inverted to obtain a PIV-like image with high-intensity signals representing particles in the flow field. The median filtering of the images aids in mitigating any noise that may get amplified due to background subtraction. Particle density of about 7–8 particles in a 32 × 32 -pixel interrogation window was observed in the data acquired. PIV and PSV data were acquired consecutively without turning off the flow in the water tunnel to avoid errors associated with slightly different flow speeds between different operations of the tunnel.

The data acquired by both PIV and PSV were processed using PIVLab (Stamhuis and Thielicke 2014; Thielicke and Sonntag 2021) with the interrogation window size starting from 128 × 128 to a final window size of 64 × 64 pixels with 50% overlap. The algorithm uses window deformation, multiple passes and recursive outlier removal and replacement. After processing the images,

Fig. 9 Schematic of the experimental setup for flow past a cylinder

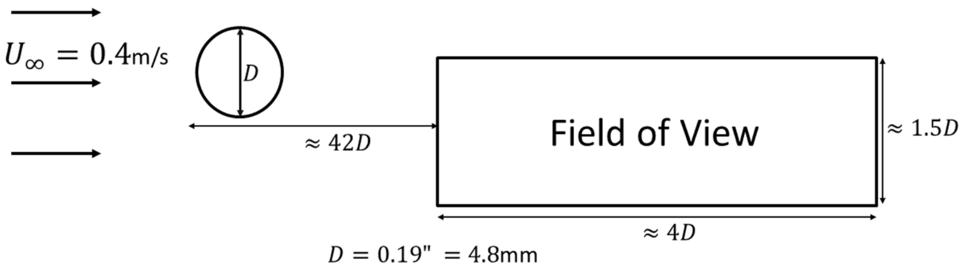

Fig. 10 Schematic of the experimental setup for boundary layer developing over a flat plate. The field of view is not to scale

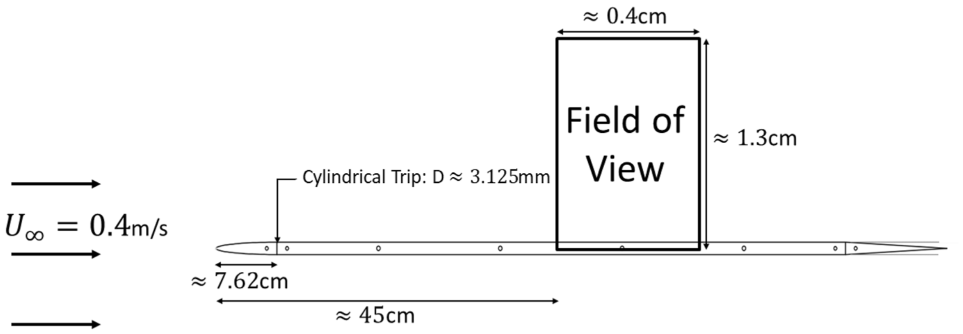

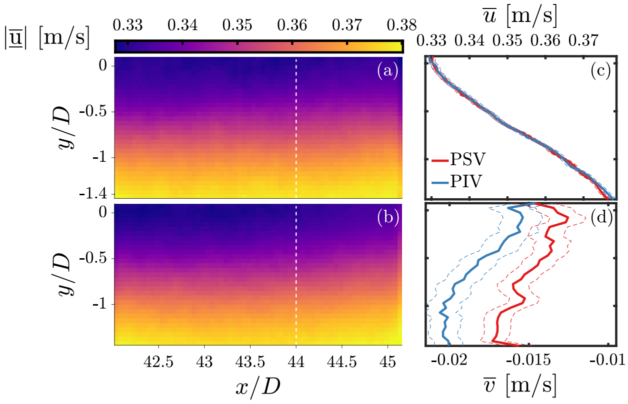

Fig. 11 Magnitude of the mean velocity field obtained from **a** PIV imaging and **b** PSV imaging. **c** and **d** Streamwise and stream-normal velocity distributions for PIV and PSV over the normalized vertical coordinate at $x/D \approx 44$

the flow statistics were computed using 2000 independent velocity fields. Figure 11 shows the mean velocity magnitude computed using (a) PIV and (b) PSV, along with mean (c) streamwise and (d) stream-normal flow velocity profiles at $x/D \approx 44$ plotted against the vertical coordinate, normalized with the cylinder diameter. The profiles in (c) and (d) are the ensemble averaged velocities obtained at the location $x/D \approx 44$. The dashed lines indicate the statistical uncertainty associated with the velocity measurements defined according to Sciacchitano and Wieneke (2016) as follows.

$$\Delta_{\overline{u}} = \frac{\sigma_u}{\sqrt{N}} \quad \text{and} \quad \Delta_{\overline{v}} = \frac{\sigma_v}{\sqrt{N}} \tag{1}$$

$\Delta_{\overline{u}}$ and $\Delta_{\overline{v}}$ are the statistical uncertainties associated with $\overline{u}$ and $\overline{v}$, respectively, σ_u and σ_v are the standard deviations of u and v, respectively, and N is the number of samples. It should be noted that these uncertainties do not account for systematic errors due to spatial modulation, pre- and post-processing, peak locking, etc. that may lead to bias in the data.

It is evident from the results shown that the preprocessed PSV images obtained work well with the cross-correlation algorithm to determine velocity fields. The PSV and PIV velocity magnitudes results are essentially identical, and the streamwise velocity shows close agreement and demonstrates the expected flow behavior with a deficit at the top of the field of view close to the wake centerline. The stream-normal velocity profiles show a small discrepancy in the magnitude, however, about 0.1 pixels on average. This disagreement between the PIV and PSV results could be due to small systematic errors in the velocity field measurements, as the difference is just outside the statistical uncertainty bounds on the measurements. The stream-normal velocity is nearly two orders of magnitude smaller than the streamwise velocity and hence is difficult to determine accurately with cross-correlation. The discrepancy is consistent across repeated experiments at the same conditions.

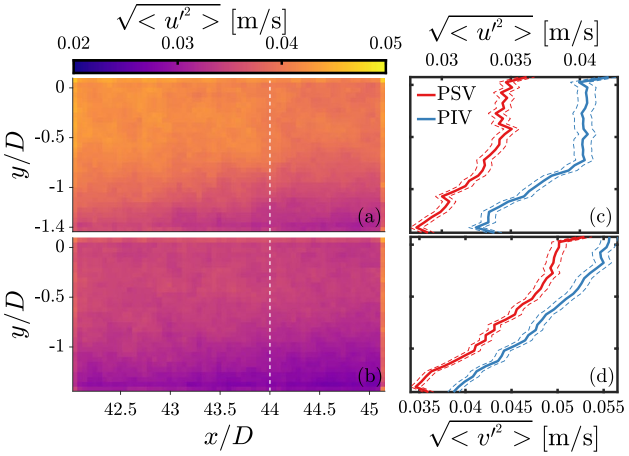

Fig. 12 Magnitude of the mean streamwise RMS field obtained from **a** PIV imaging and **b** PSV imaging. **c** and **d** Streamwise and stream-normal RMS distributions for PIV and PSV at $x/D \approx 44$ over the normalized vertical coordinate

Second-order velocity statistics were also computed from the velocity fields obtained from PIV and PSV. Figure 12 shows the magnitude of the streamwise RMS velocity computed using (a) PIV and (b) PSV, along with (c) streamwise and (d) stream-normal RMS velocity profiles at $x/D \approx 44$ traced against the stream-normal coordinate normalized by the diameter of the cylinder. The statistical uncertainty is plotted as dashed lines and is defined as follows according to Sciacchitano and Wieneke (2016).

$$\Delta_{\overline{u'^2}} = \overline{u'^2}\sqrt{\frac{2}{N}} \quad \text{and} \quad \Delta_{\overline{v'^2}} = \overline{v'^2}\sqrt{\frac{2}{N}} \tag{2}$$

$\Delta_{\overline{u'^2}}$ and $\Delta_{\overline{v'^2}}$ are the statistical uncertainties associated with the streamwise and stream-normal RMS velocities, $\overline{u'^2}$ and $\overline{v'^2}$, respectively, and N is the number of samples. While the general trend in RMS agrees between PIV and PSV, there is a discrepancy in the magnitude of the RMS velocity of 0.35 and 0.32 pixels for the streamwise and stream-normal components, respectively, with PSV producing lower-magnitude fluctuations.

The cause of this discrepancy is not immediately clear, and it may be the result of several factors. While it cannot be ruled that part or all of the discrepancy is due to an effect inherent to PSV, such as depth of field effects, it is entirely possible that the processing algorithm and preprocessing of the images play a significant role. It is known that different preprocessing routines on image data can have a strong effect on higher-order statistics. To demonstrate this, both the PSV and PIV images were preprocessed through a Gaussian filter of 3 × 3 pixels in size, and were then processed using the same algorithms to obtain the velocity fields. The RMS velocity results are shown in Fig. 13.

Figure 13 shows the (a) streamwise and (b) stream-normal RMS velocity profiles computed using PIV and PSV images, processed with and without preprocessing through a Gaussian filter. Preprocessing the images through a Gaussian filter changes the magnitude of the RMS for the same set of images, illustrating the sensitivity of higher-order statistics to preprocessing. The RMS magnitude is consistently higher for PIV compared to PSV, however, indicating that there is likely at least a small effect present inherent to the imaging setups. The correlation coefficients were calculated using PIVLab to explore this further (Thielicke and Sonntag 2021; Raffel et al. 2018). Figure 14 shows a histogram of the correlation coefficients obtained for 2000 velocity vectors for all 2048 interrogation windows, for both PSV and PIV, with and without Gaussian filtering of the images. As expected, the quality of correlation is enhanced by the use of a Gaussian filter to preprocess the images. More importantly, the results show that PSV is capable of achieving correlation quality equivalent to that of PIV. However, this increase in correlation quality might not necessarily translate to an increased accuracy in velocity measurements. Hence, whether the discrepancy in RMS represents additional noise in the PIV data compared to PSV or a reduction in sensitivity of PSV to real velocity fluctuations cannot be determined definitively without a ground truth to compare against.

3.2.2 Boundary layer

PSV and PIV imaging were also performed in a boundary layer developing over a flat plate at a Reynolds number of $Re_{\delta_{99}} = 6.1 \times 10^3$ with $\delta_{99} = 2$ cm. Frames (a), (b) and (c) of Fig. 15 show, respectively, a raw PSV image, the same image after applying preprocessing and a PIV image captured at the same focal plane in the same flow during the same experimental run as PSV. Only the portion closest to $y = 0$ is shown to highlight scattering from the wall. As in Sect. 3.2.1, PSV captures approximately the same particle seeding density as PIV of about 7-8 particles in a 32 × 32 -pixel interrogation window. The wall is located at $y = 0$, and a small amount of light scattering is visible there in the PIV image shown in Fig. 15c even after wall intensity subtraction (i.e., subtracting the mean of the wall scattering from individual frames) and the use of a physically transparent wall, whereas the PSV data shown in Fig. 15b exhibit no such artifacts.

The particle images acquired by both PIV and PSV were again processed using PIVLab (Stamhuis and Thielicke 2014; Thielicke and Sonntag 2021) with the interrogation window size starting from 128 × 128 to a final window size of 32 × 32 pixels with 50% overlap. After processing the images, the flow statistics were computed using 2000

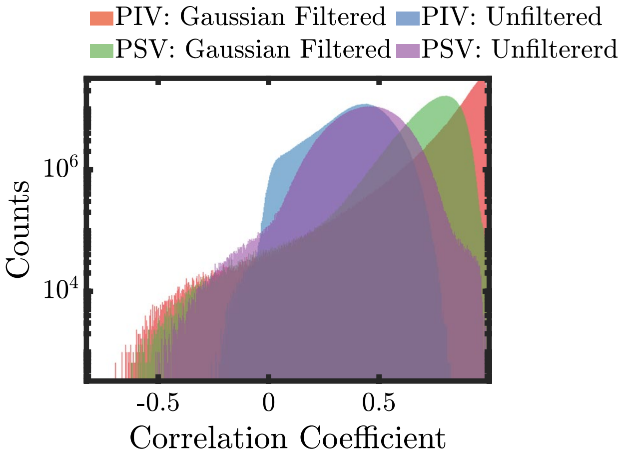

Fig. 14 Correlation coefficient for PIV and PSV results obtained with and without preprocessing through a Gaussian filter

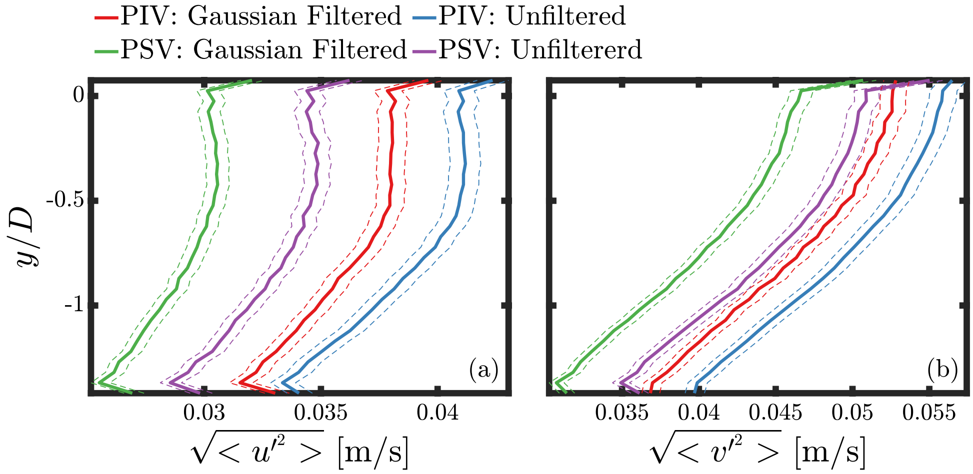

Fig. 13 **a** Streamwise and **b** stream-normal RMS velocity distributions obtained by PSV and PIV with and without preprocessing through a Gaussian filter

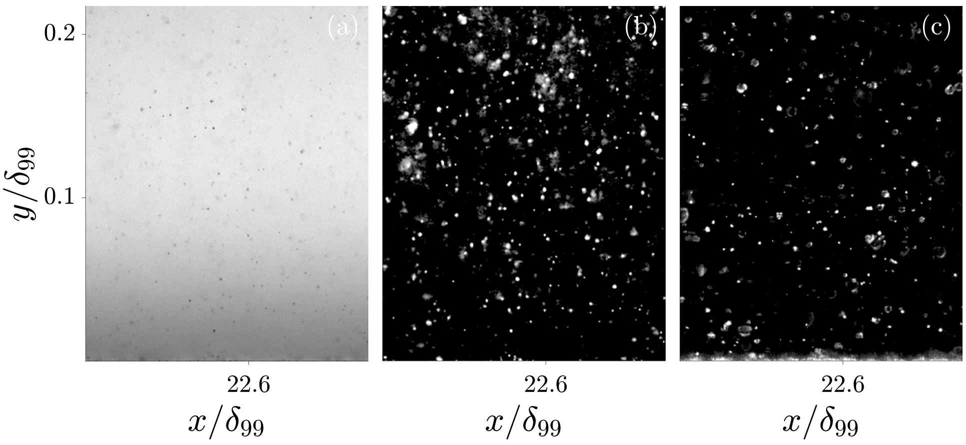

Fig. 15 **a** Raw PSV image (contrast-enhanced for better visualization), **b** the same image after preprocessing applied, **c** PIV image captured in the same flow at the same focal plane

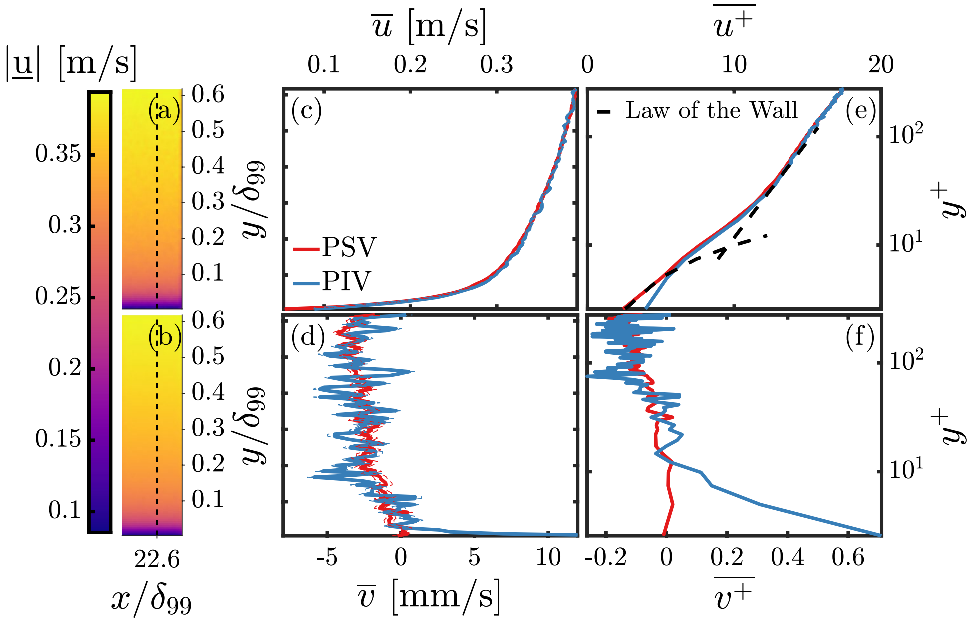

Fig. 16 Magnitude of the mean velocity field obtained from **a** PIV imaging and **b** PSV imaging. **c** and **d** Streamwise and wall-normal velocity distributions for PIV and PSV at $x/\delta_{99} = 22.5$ over the normalized vertical coordinate. **e** and **f** Magnitude of the mean streamwise and wall-normal velocity field in viscous units

independent velocity fields. Figure 16 shows the mean velocity magnitude computed using (a) PIV and (b) PSV, along with mean (c) streamwise and (d) wall-normal flow velocity profiles at $x/\delta_{99} = 22.5$ plotted against the vertical coordinate normalized with the boundary layer thickness, δ_{99}, where the dashed lines indicate the statistical uncertainty associated with the velocity measurements defined in Eq. 1. The mean PSV and PIV velocity magnitudes results agree well with each other, and both the streamwise and wall-normal components obtained from PSV show excellent agreement with PIV measurements within the expected uncertainty interval. It is noted that the streamwise velocity goes to zero near the wall as expected for PSV, while it does not for PIV data, likely due to interference from the wall reflections. The result for the wall-normal component is similar, and the profile for PSV appears to be better resolved.

Figure 16e and f shows the mean streamwise and wall-normal velocity profiles obtained from PSV and PIV in viscous units. As the PSV results appear to be better resolved in Fig. 16, they were used to determine the friction velocity u_τ and the viscous length scale δ_ν for the normalization of the velocity profiles. The friction velocity was found to be 0.0169 m/s and one viscous unit was found to be 60 μm, which is equivalent to about 9 pixels per viscous wall unit. The law of the wall for the mean streamwise velocity is plotted as the dashed black curve, showing excellent agreement with the PSV results in the viscous sublayer $y^+ \leq 5$.

The constant C^+ in the law of the wall (Eq.) 3 was found to be 4, which is lower than the theoretical value of 5 for smooth walls (Pope 2001; Marusic et al. 2010).

$$u^+ = \frac{1}{\kappa} \ln y^+ + C^+, \text{where } \kappa \approx 0.41 \tag{3}$$

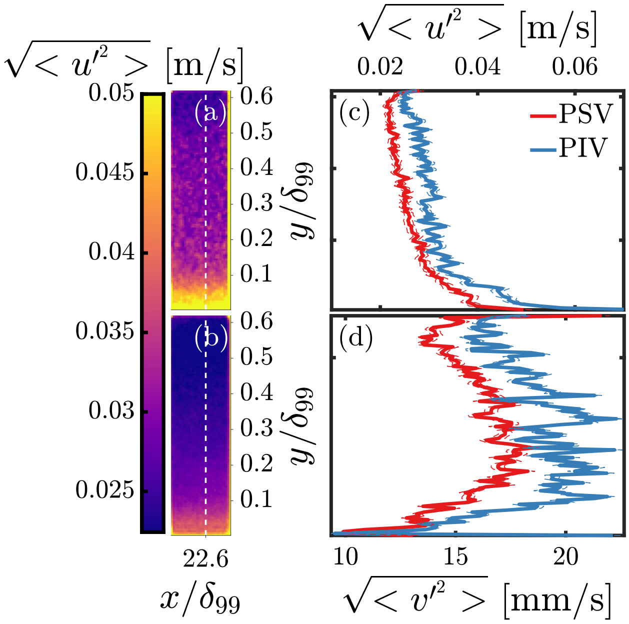

Fig. 17 Magnitude of the mean streamwise RMS field obtained from **a** PIV imaging and **b** PSV imaging for a turbulent boundary layer. **c** and **d** Streamwise and wall-normal RMS distributions for PIV and PSV at $x/\delta_{99} = 22.5$ over the normalized vertical coordinate

To further compare the two techniques, second-order velocity statistics were also computed from the velocity fields obtained from PIV and PSV. Figure 17 shows the magnitude of the streamwise RMS velocity computed using (a) PIV and (b) PSV, along with (c) streamwise and (d) wall-normal RMS velocity profiles plotted against the wall-normal coordinate, normalized by δ_{99}. The statistical uncertainty is plotted as dashed lines as defined in Eq. 2. As observed in Sect. 3.2.1, while the trends agree, there is a discrepancy in the magnitude of the RMS velocity, and the RMS is again higher for the PIV measurements. The discrepancy is about 0.1 pixels and 0.07 pixels for the streamwise and wall-normal components, respectively, in terms of the displacements of the flow tracers. Analysis of the data with Gaussian filtering applied to the images and examining the correlation coefficients yields essentially identical findings as those discussed for the cylinder wake and presented in Figs. 13 and 14.

4 Conclusions

Particle shadow velocimetry (PSV) is explored as a laser-free alternative to particle image velocimetry (PIV). PSV provides several potential advantages over PIV such as better near-wall and near-interface particle imaging, laser-free operation and cost-effectiveness, but its performance compared to PIV was not well studied. Section 2 shows that PSV is capable of achieving similar seeding density as PIV in the same experimental setup, and that the depth of field of a PSV system, while larger than what is possible with PIV, still falls within the range of typical values encountered in PIV. PSV and PIV were compared in two experimental configurations: flow past a cylinder and boundary layer over a flat plate in a water tunnel. Both PIV and PSV experiments were conducted at the same plane in the same experimental run. The flow statistics obtained from PSV under both the experiments show close agreement with PIV results in the mean, while the RMS velocity is slightly lower with PSV compared to PIV in both experiments. It may be possible to resolve the discrepancy by modifying the preprocessing routine or processing parameters in the velocimetry algorithm, but it is not clear which measurement (or neither) is correct because there is no ground truth to compare against. It is possible that the slightly larger depth of field of PSV plays into this discrepancy. The larger depth of field may play a significant role in flows with appreciable three-dimensional motion as it can potentially lead to undesired averaging of the spatial scales.

PSV is not without its limitations, however. Because PSV requires collimated light, the maximum field of view is limited to the size of the collimated light beam, which is typically much smaller than the field of view possible in a PIV setup. In addition, the apparent particle image size is highly dependent on the physical size of the tracer particles and the magnification of the system. This would likely cause difficulties in applications in gases, where the particles are typically more than an order of magnitude smaller than those used in liquids, or where the field of view is large. In those cases, the particle images would likely not be large enough to be processed effectively.

Acknowledgements The authors would like to acknowledge the financial support by the National Science Foundation under Grant No. CBET-2306815.

References

Estevadeordal J, Goss L (2005) Piv with led: particle shadow velocimetry (psv) technique. In: 43rd AIAA Aerospace Sciences Meeting and Exhibit, p. 37

Goss L, Estevadeordal J, Crafton J (2007) Velocity measurements near walls, cavities, and model surfaces using particle shadow velocimetry (psv). In: 2007 22nd International Congress on Instrumentation in Aerospace Simulation Facilities, pp. 1–8. IEEE

Hessenkemper H, Ziegenhein T (2018) Particle shadow velocimetry (psv) in bubbly flows. Int J Multiphase Flow 106:268–279

Khodaparast S, Borhani N, Tagliabue G, Thome JR (2013) A micro particle shadow velocimetry (μpsv) technique to measure flows in microchannels. Exper Fluids 54:1–13

Khodaparast S, Borhani N, Thome J (2014) Application of micro particle shadow velocimetry μpsv to two-phase flows in microchannels. Int J Multiphase Flow 62:123–133

Marusic I, McKeon BJ, Monkewitz PA, Nagib HM, Smits AJ, Sreenivasan KR (2010) Wall-bounded turbulent flows at high reynolds numbers: recent advances and key issues. Phys Fluids 22(6):065103

Paterna E, Moonen P, Dorer V, Carmeliet J (2013) Mitigation of surface reflection in piv measurements. Measurement Sci Technol 24(5):057003

Pope SB (2001) Turbulent flows. Measurement Sci Technol 12(11):2020–2021

Raffel M, Willert CE, Scarano F, Kähler CJ, Wereley ST, Kompenhans J (2018) Particle image velocimetry: a practical guide. Springer, Cham

Schmidt BE, Sutto JA (2019) High-resolution velocimetry from tracer particle fields using a wavelet-based optical flow method. Exp Fluids. https://doi.org/10.1007/s00348-019-2685-6

Schmidt BE, Sutton JA (2020) Improvements in the accuracy of wavelet-based optical flow velocimetry (wOFV) using an efficient and physically based implementation of velocity regularization. Exp Fluids. https://doi.org/10.1007/s00348-019-2869-0

Sciacchitano A, Wieneke B (2016) Piv uncertainty propagation. Measurement Sci Technol 27(8):084006

Stamhuis E, Thielicke W (2014) Pivlab-towards user-friendly, affordable and accurate digital particle image velocimetry in matlab. J Open Res Softw 2(1):30

Thielicke W, Sonntag R (2021) Particle image velocimetry for matlab: accuracy and enhanced algorithms in pivlab. J Open Res Softw. https://doi.org/10.5334/jors.334

Willert CE, Mitchell DM, Soria J (2012) An assessment of high-power light-emitting diodes for high frame rate schlieren imaging. Exp Fluids 53(2):413–421

Willert C, Stasicki B, Klinner J, Moessner S (2010) Pulsed operation of high-power light emitting diodes for imaging flow velocimetry. Measurement Sci Technol. https://doi.org/10.1088/0957-0233/21/7/075402